A study on tectonic and sedimentary development in the rifted northern continental margin of the South China Sea near Taiwan

Wei-Zhi Liao[1], Andrew T. Lin[2], Char-Shine Liu[3], Jung-Nan Oung[4], and Yunshuen Wang[5]

Abstract

A series of Cenozoic rifted basins developed in the northern margin of the South China Sea (SCS). Tainan Basin is one of these rifted basins near Taiwan, lying in the outer margin. We have used reflection seismic data in the deepwater areas and boreholes drilled in the shelf of the Tainan Basin to understand the tectonic and sedimentary development in the northern SCS margin near Taiwan. Four key stratal surfaces (i.e., the base of the Pleistocene Series, the base of the Pliocene Series, the 17 Ma maximum flooding surface [MFS], and a breakup unconformity of approximately 30 Ma in age) and seven seismic facies (i.e., continuous- and parallel-layer seismic facies, wavy seismic facies, chaotic seismic facies, U-shaped canyon-cut seismic facies, imbricated-layer seismic facies, high-amplitude reflector package seismic facies, and extrusive volcanism seismic facies) are recognized from seismic data with ages constrained by borehole stratigraphy drilled in the shelf. We have established a model for Cenozoic tectonic and sedimentary development in the rifted northern margin of the SCS near Taiwan. The occurrence of Paleogene fault-bounded grabens/half-grabens topped by a breakup unconformity and draped by postrift sediments indicates that these deepwater rifted basins developed on the continental crust, attesting that a thinned continental crust underlies the deepwater study area, rather than oceanic crust as reported in some literature. Postbreakup extrusive volcanic bodies, of early Miocene age, were buried by thick deepwater sediments. Fairly continuous stratal surfaces of 17 Ma MFS reveal that volcanic activities ceased to be active since middle Miocene. A series of channel cut-and-fills is observed in late Miocene, Pliocene, and Pleistocene strata beneath and to the south of the modern Formosa Canyon. Two distinct fields of deepwater sediment waves developed since middle Pleistocene are found lying to the west of modern deformation front/Manila Trench and to the north and south of the Formosa Canyon, respectively.

Introduction

The rifting of South China started in Jurassic times (Li, 2000), whereas the South China Sea (SCS) oceanic spreading occurred during the late Oligocene to mid-Miocene (Taylor and Hayes, 1983; Briais et al., 1993; Barckhausen et al., 2014). Tainan Basin, a Tertiary rifted basin, is one of the rifted basins that developed in the northern SCS continental margin (Yang et al., 1991; Lee et al., 1993; Tzeng et al., 1996; Lin et al., 2003). The northeastern deepwater area of the SCS lies to the south of the Tainan Basin. Sibuet et al. (2002) indicate that there is a piece of oceanic crust lying beneath the northeastern corner of the SCS. Magnetic evidence from this area suggests that a plate boundary, called the Luzon Ryukyu Transform Plate Boundary (LRTPB in Figure 1), could be interpreted to divide the SCS oceanic crust to the west

from the distal Philippine Sea oceanic crust in the east and beneath the northeastern corner of the SCS (Sibuet et al., 2002; Hsu et al., 2004). However, crustal velocity and grabens seen from high-quality reflection seismic data suggest that continental crust lies beneath the deep-water area in the northeastern corner of the SCS (McIntosh et al., 2013, 2014; Lester et al., 2014).

Key stratal surfaces and unconformities in Cenozoic strata (e.g., breakup unconformity) have been interpreted and correlated on reflection seismic data from drilled stratigraphy at boreholes in the margin (e.g., Ocean Drilling Program (ODP), Integrated Ocean Drilling Program (IODP, 2003–2013), and International Ocean Discovery Program (IODP, 2013~) sites and hydrocarbon exploration wells in the Pearl River Mouth Basin and the Tainan Basin) (Li et al., 2007, 2015;

[1]National Central University, Department of Earth Sciences, Taiwan and National Taiwan University, Institute of Oceanography, Taiwan. E-mail: jason.weizhi.liao@gmail.com.

[2]National Central University, Department of Earth Sciences, Taiwan. E-mail: andrewl@ncu.edu.tw.

[3]National Taiwan University, Institute of Oceanography, Taiwan. E-mail: csliu@ntu.edu.tw.

[4]CPC Corporation, Taiwan. E-mail: oungin@cpc.com.tw.

[5]Central Geological Survey, MOEA, Taiwan. E-mail: wangys@moeacgs.gov.tw.

Yeh et al., 2010; Lester et al., 2014; McIntosh et al., 2014; Li et al., 2015). For example, we correlated the 17 Ma maximum flooding surface (MFS) from the shelf Tainan Basin because this stratal surface is well-correlated in the postbreakup stratigraphy beneath western Taiwan and the Taiwan Strait as reported in Lin (2001). These studies also pointed out that many buried grabens and volcanos developed in early and middle Cenozoic. There is an emergent volcano, herein called the Formosa seamount, which stands out above the seafloor in the study area (Figure 1), and age datings from the dredged basalt show that the basaltic rock is of the age of approximately 21–22 Ma (Wang et al., 2012). However, there has been no detailed study to constrain the age of other buried volcanos, igneous rock, and other sedimentary features in the northeastern deepwater region of the SCS.

The objective of this study is to understand the evolution of Cenozoic tectonic and sedimentary development in the northeastern deepwater area of the SCS near Taiwan. Analyses of seismic sequence and seismic facies are carried out in this study. A Cenozoic tectonic and sedimentary development model in the study area is proposed by integrating these results.

Regional geologic setting

The study area lies to the west of the deformation front and the Manila Trench of the Manila subduction zone and to the east of the Dongsha Slope in a water depth ranging from outer shelf in the north to approximately 4000 m water depth in the south (Figure 1). Morphologically, the study area is characterized by a northeast-trending Dongsha Slope and an east–west-trending Tainan Slope in the northeast and northwest, respectively. The gradient of the slope is approximately 2%–3% with bathymetric ridges and gullies running perpendicular to the strike of the slope. In the south, it is characterized by the base of the slope and a deepwater area of 2600–3600 m in depth with a gentle slope (less than 0.2°). A major submarine canyon, the Formosa Canyon (called the Taiwan Canyon by Zhong et al., 2015), forms an approximate boundary between the Dongsha Slope and the Tainan Slope. This canyon turns to an east–west direction at the base of slope and runs eastwardly to join the north–northwest-trending Penghu Canyon in the east, which lies along the deformation front. The confluence of the Formosa Canyon and the Penghu Canyon then joins southwardly to the Manila Trench, which, again, lying in front of the north-north-west-trending deformation front. To the east of the deformation front, the area is termed Kaoping Slope, pertaining to a fold-and-thrust belt consisting of accreted sediments above the decollement thrust (Figure 1). Two types of sediment wavefields are observed at both sides of the lower reach of the Formosa Canyon and to the west of the Penghu Canyon (Damuth, 1979; Gong et al., 2012, 2015; Kuang et al., 2014). The upper slope, especially the Formosa Ridge and the Jiulong Ridge, is investigated in detail by the Taiwan Gas Hydrate Research Team (e.g., Chen et al., 2014; Liao et al., 2014).

A Paleogene-rifted basin, the Tainan Basin, developed in the northeastern SCS margin in the north of the study area. There are three tectonic elements in this basin: northern depression, central uplift zone, and southern depression (Figure 1; Tsao et al., 1992, Lin et al.,
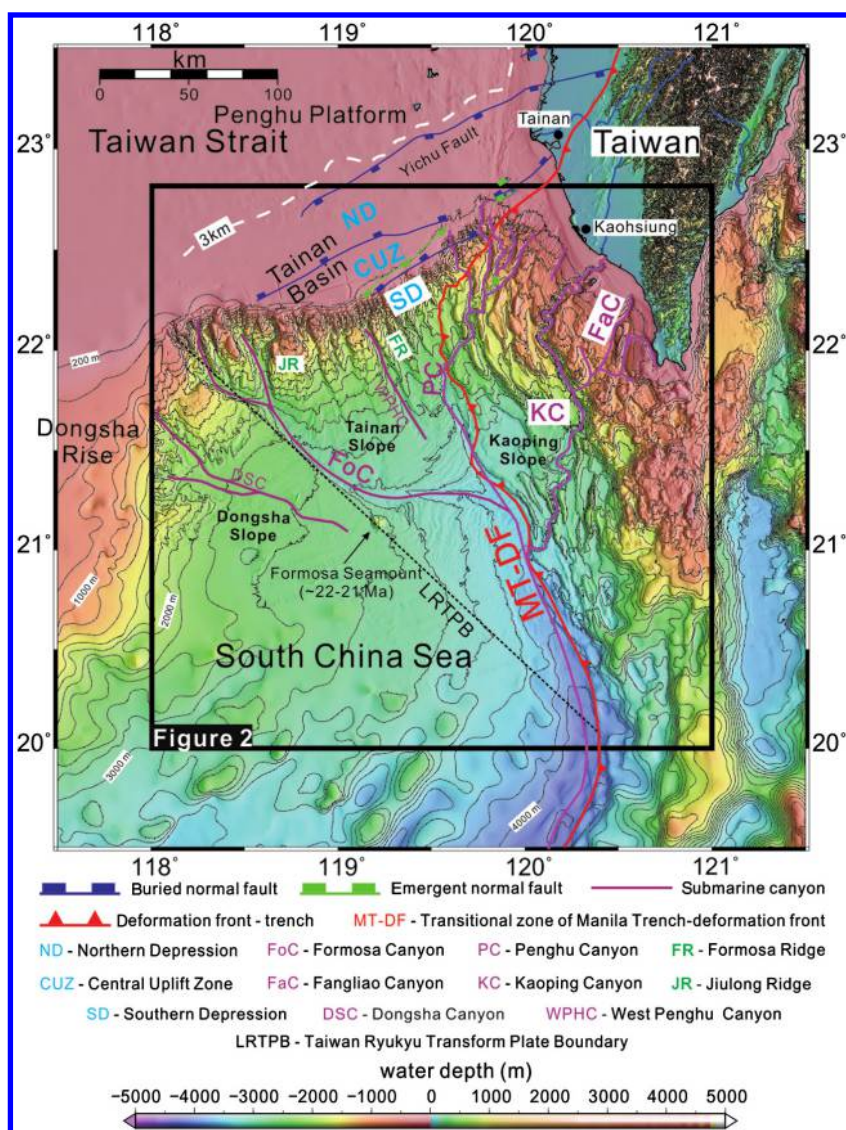

Figure 1. Bathymetry and tectonic features off southwest Taiwan. Tectonic elements and sediment isopach of 3 km marked as a white dashed line in the Taiwan Strait are from Lin et al. (2003). The age of Formosa Seamount is from Wang et al. (2012). Purple lines are the courses of submarine canyons.

2003). The northern depression, central uplift zone, and a part of the southern depression lie in the shelf region (Yang et al., 1991; Lee et al., 1993; Tzeng et al., 1996; Tang et al., 1999; Lin et al., 2003), whereas the rest of the southern depression lies in the slope region (Figure 1). A series of east-northeast-trending normal faults developed in the shelf (Yang et al., 1991) with one major north-dipping, graben-bounding fault lying in the upper continental slope in the western part of the southern depression (Li et al., 2007; Lester et al., 2012; Yeh et al., 2012). However, Li et al. (2007) and Lester et al. (2012) assume that this fault is the northern boundary of the central uplift zone. Our data show that this fault is not the northern boundary fault for the central uplift zone, but a fault in the southern depression. Another important fault is a south-dipping fault in the outer shelf and near the shelf break in the eastern part of the Tainan Basin (Lin et al., 2008). A seafloor fault scarp (approximately 50 m offset), rotated hanging-wall strata, and stratal truncation beneath the upper slope indicate that this emergent fault is a major and active growth normal fault (Lin et al., 2003, 2008). Lin et al. (2008) divide the Tainan Slope into an eastern and a western part with the fault pertaining to the eastern part of the slope.

The Taiwan mountain belt has developed since approximately 6.5 Ma, and this collisional belt has overridden the rifted continental margin (Lin et al., 2003). A series of folds and thrusts extends from the subaerial mountain belt to the submarine accretionary wedge on the Kaoping Slope. The deformation front, which indicates the western limit of the compressional structures, delimits the accretionary wedge in the east and the incoming and subducting rifted continental margin in the west. In the west, a bathymetric high of rhomboid shape, called Dongsha Rise, separates the Tainan Basin and the Pearl River Mouth Basin (Nissen et al., 1995; Ludmann and Wong, 1999; Ludmann et al., 2001). The SCS deep-sea basin locates to the south of the study area and is floored by oceanic crust. The duration for the oceanic spreading of the SCS as determined by magnetic anomalies is of late Oligocene to mid-Miocene age (Taylor and Hayes, 1983; Briais et al., 1993; Barckhausen et al., 2014).

Data and methods

To identify the tectonic and sedimentary developments in the SCS near Taiwan, borehole data, and reflection seismic data were collected in the northeastern SCS. Data from two hydrocarbon exploration boreholes, A-1 and JA-1, and seismic profiles across these two boreholes are from CPC Corporation, collected in the outer shelf of the western Tainan Basin (Figure 2). Two grids of reflection seismic data collected as part of the Taiwan Integrated Geodynamic Research (TAIGER) project and the Taiwan Gas Hydrate Research Project, respectively, are used in this study. The large-offset seismic data (MGL0905 seismic data in Figure 2), which were collected by using *R/V Marcus G. Langseth* in May 2009 under the scope of the TAIGER project. The streamer

length is approximately 6000 m with 468 hydrophone channels at a 12.5 m group spacing. The source is a 6600 in.[3] array consists of four subarrays of mixed air guns. The shot interval is fixed at 50 m. Other multichannel seismic (MCS) data were collected by using *R/V Ocean Researcher I* in 2012 (MCS994, MCS1000, and MCS1014) and 2013 (MCS1046) as part of gas hydrate studies funded by the Central Geological Survey, Taiwan. The acquisition parameters for these MCS data are as follows: 1500 m streamer length and 108 hydrophone channels with 12.5 m group spacing. The source is approximately 1000 in.[3] array and consists of three air guns. Both seismic grids of MGL0905 and MCS data were processed using the ProMax and Echos softwares at the Institute of Oceanography, the National Taiwan University.

There are four key stratal surfaces: base of the Pleistocene Series, base of the Pliocene Series, mid-Miocene MFS, and the breakup unconformity, being recognized in this study, and we are able to correlate them from the shelf to the deep-sea region in the northeastern SCS margin. Analyses on seismic facies were also performed on these seismic data. With the help of sequence correlations and seismic facies analyses, we are able to propose a tectonic and sedimentary development model for the Cenozoic-rifted continental margin of the northeastern SCS near Taiwan.

Results
Tectonic and sedimentary features

Volcanic seamounts (Figures 3, 4, and 5), grabens (Figure 6), paleocanyon features (including lateral accretion [Figure 7] and canyon cut-and-fill features [Figure 8]), and sediment waves (Figure 8) commonly appear in the study area. A series of buried volcanic seamounts lie in the eastern part of the study area and near the Penghu Canyon/Manila Trench. The heights of these buried seamounts are more than 500 m (0.5 s two-way traveltime [TWT], Figure 4) above the surrounding basement. Features flanking the seamounts interpreted as relating to volcanic activities (e.g., lava flows and sills), shown as low-frequency and high-amplitude reflectors, are also found. However, a small group of emergent volcanic seamounts stands a little distance away south of the Formosa Canyon and surpasses the seafloor over 1000 m (Figure 3). The cone-shaped volcano, volcanic sills, and lava-flow characteristics can be clearly identified on seismic profiles in the proximal area of this seamount group. Grabens are also observed in the deepwater area with thick graben infills. The Oligocene breakup unconformity separates the underlying graben infills, interpreted as Paleogene syn-rift sequences, from overlying younger postbreakup cover sediments. Most of the grabens are confined by graben-bounding normal faults on one or both sides of grabens and the horst features can also be observed (Figure 6). However, tilted reflectors and divergent reflections of graben infills show that a few grabens are affected by normal faulting and episodic faulting activities (Figure 6).

A series of canyon cut-and-fill features are present under the deepwater area near the Formosa Canyon and Penghu Canyon/Manila Trench (Figure 8). The U-shaped and eroded valleys are contained with infills showing parallel and chaotic reflections. A series of shingled reflections are observed beneath modern Formosa Canyon (Figure 7). Sediment wavefields are also observed on the seafloor to the north and south of the lower reach of the Formosa Canyon in the study area. Stratal thickness for these sediment waves is more than 100 m.

Seismic facies of the Neogene strata

According to characteristics of seismic reflectors, seven major seismic facies are identified for the Neogene strata (Table 1; Figures 3–8): (1) seismic facies A: continuous and parallel reflection configuration, (2) seismic facies B: wavy and continuous reflection configuration, (3) seismic facies C: chaotic reflection configuration, (4) seismic facies D: U-shaped and canyon-cut reflection configuration, (5) seismic facies E: shingled reflection configuration, (6) seismic facies F: high-amplitude reflector packages (HARP) reflection
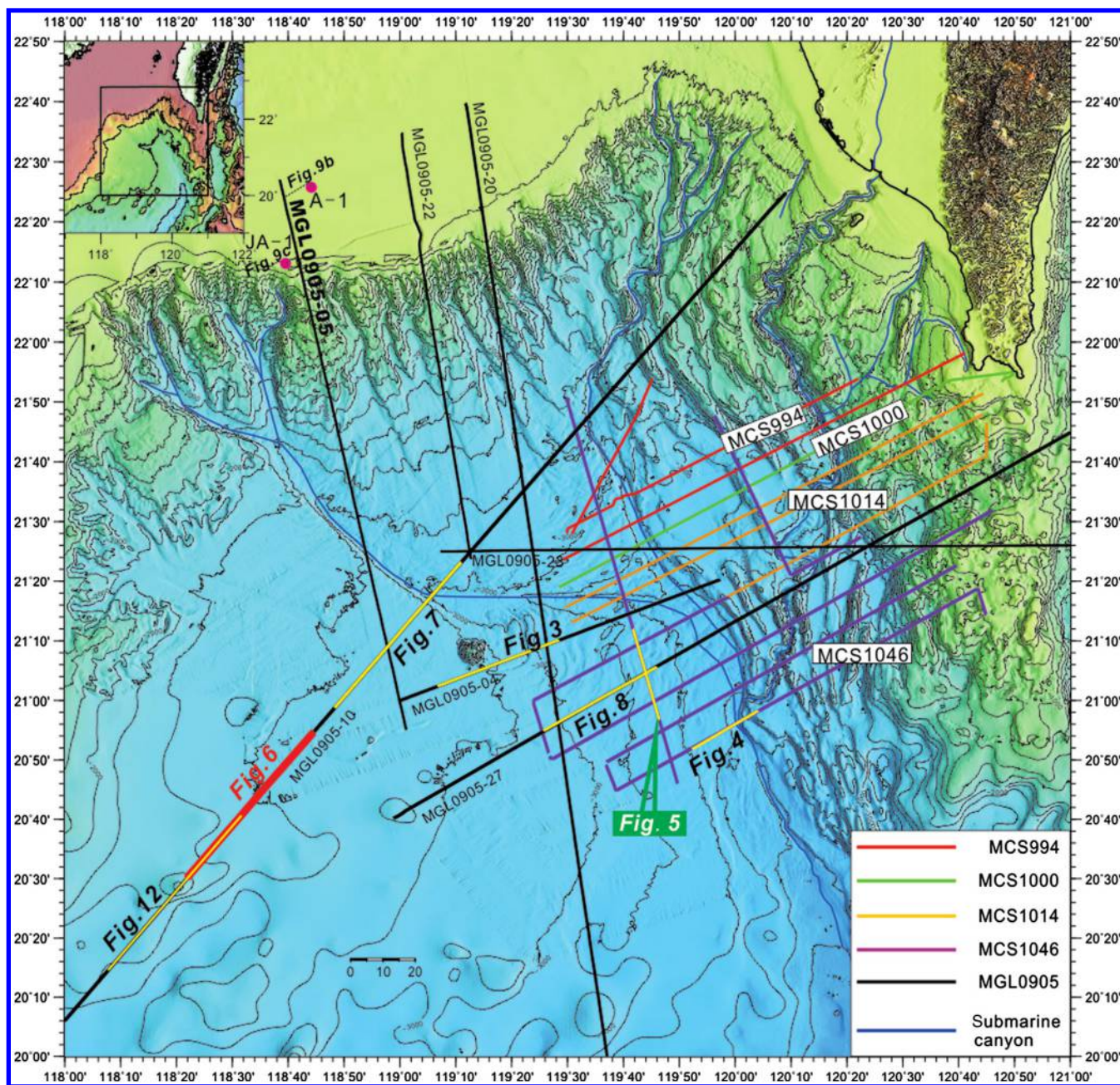

Figure 2. Shaded relief map with contours off southwestern Taiwan. Colored solid lines represent grids of seismic data used in this study. Key stratal surfaces correlating from A-1 and JA-1 boreholes in the shelf to MGL0905-05. Yellow lines show the location of figures. Stratigraphic correlation from boreholes A-1 and JA-1 to MGL0905-05 line can be found in Figure 9.

configuration, and (7) seismic facies G: discontinuous, high-amplitude and low-frequency reflection configuration. The seismic facies and their interpretations are described below.

Seismic facies A: Continuous and parallel reflection configuration

Seismic facies A appears widely in the Neogene strata (Figures 3–8). It generally shows good continuity and parallel reflectors in the seismic profile. The amplitude is relatively strong in the shallow section and becomes weaker for deeper reflections due to amplitude attenuation with increasing depths. The low-amplitude and continuous reflectors are interpreted as hemipelagites accumulated from suspension, whereas the higher amplitude and continuous reflections may result from interbeds of hemipelagites and coarser grained turbidites deposited in the channels and overbanking areas
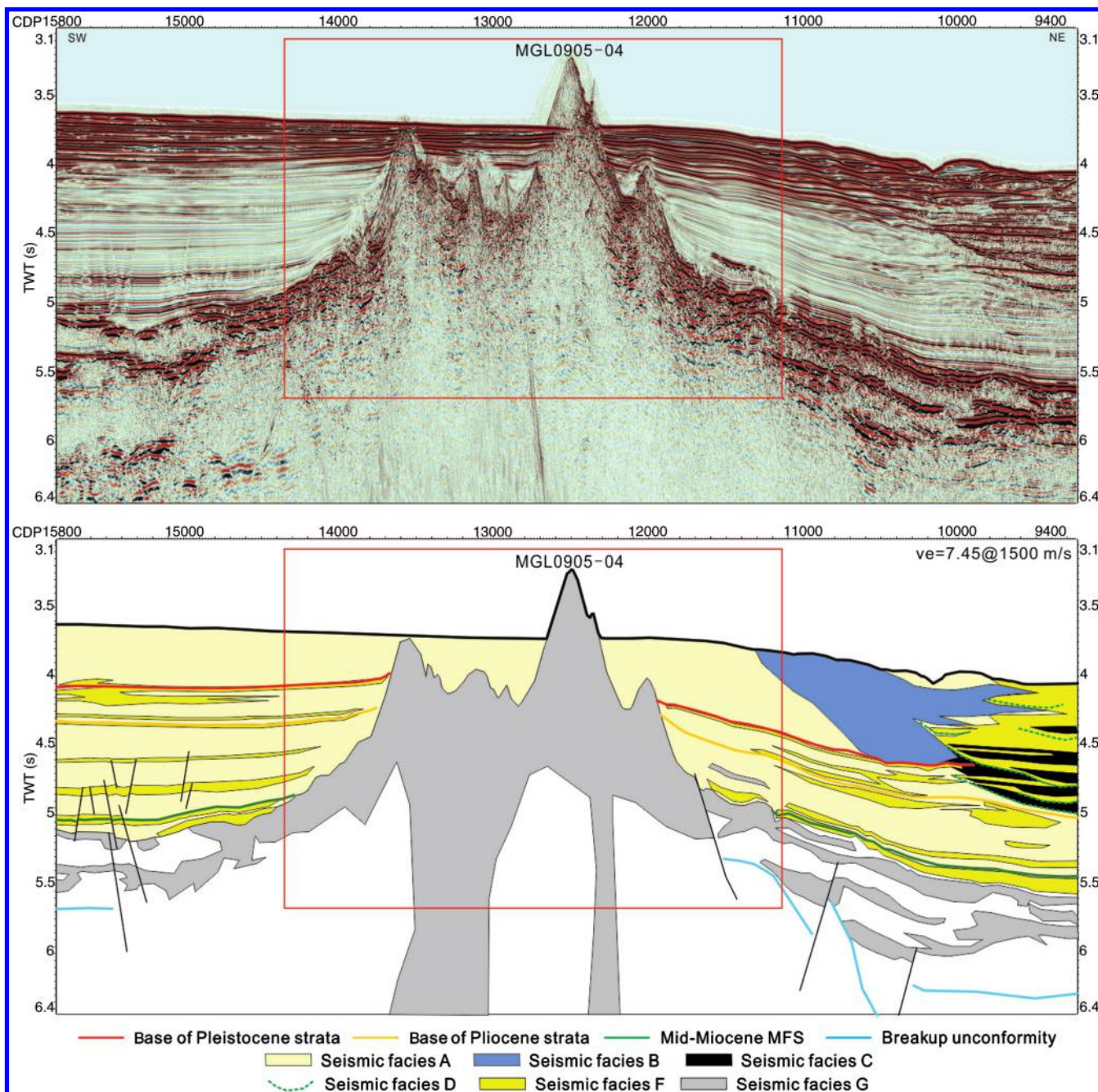
Figure 3. Seismic section and its interpretation of MGL0905-04, showing the volcano group in the central part of the study area. This volcano group and its lateral equivalents (lava flows and sills) are shown as low-frequency, high-amplitude reflections in this profile. Possible conduits of extrusive volcanic lavas beneath the volcanos are also drawn. Part of the Formosa Canyon infills is also revealed in this profile. Red rectangular displays the buried and emergent volcano group. See Figure 2 for profile location.

analogous to similar reflection configurations that have been drilled during IODP Expedition 349, for example, at site U1431 (Li et al., 2015).

Seismic facies B: Wavy and continuous reflection configuration

Seismic facies B has developed since the late Quaternary and underlain the seafloor to the north and south of the lower reach of the Formosa Canyon and to the west of the Penghu Canyon/Manila Trench. In some places, this seismic facies mostly overlies seismic facies C or F (see below; Figures 3, 4, 5, 7, and 8). This seismic facies is interpreted as deepwater sediment waves similar to those found in many other places in the world (e.g., Ediger et al., 2002; Lewis and Pantin, 2002; Lom-keil et al., 2002; Mosher and Tomson, 2002; Wynn and Stow, 2002). The sediment waves are high-amplitude reflectors and can be divided into two sediment wavefields according to the wavelength and reflector continuity (Gong et al., 2012, 2015; Kuang et al., 2014). The wavelength
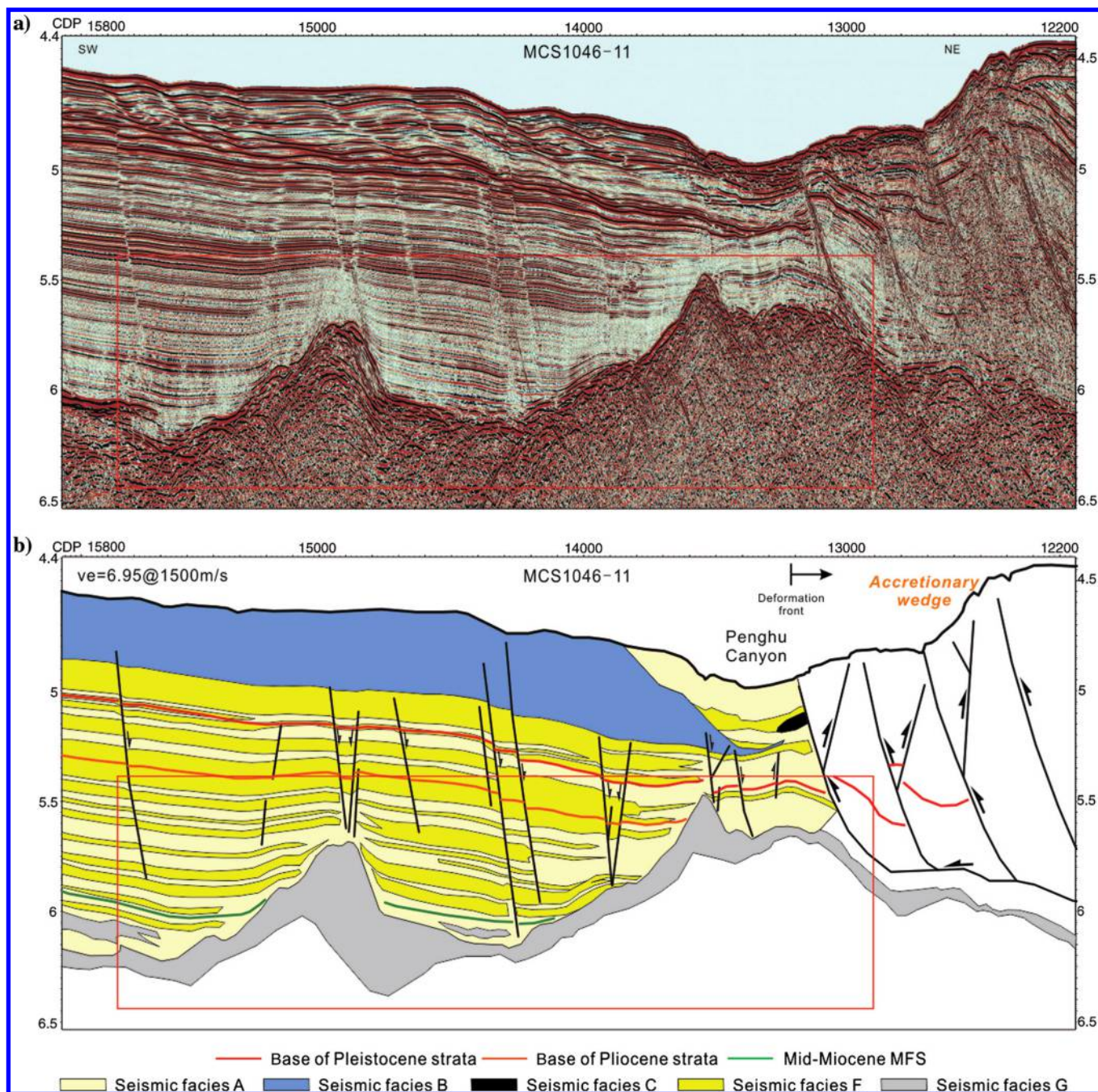
Figure 4. Seismic section of MCS1046-11 (a) and its interpretation (b). This seismic profile shows buried seamounts in the southeast of the study area lying in the distal margin and in front of approaching accretionary wedge. The abundant HARP facies indicate thick turbidites in this region. Red rectangular outlines the buried seamounts. The arrows indicate the displacement direction of the faults. Profile location is shown in Figure 2.

is approximately 2000–4000 m measured from bathymetric map and wave height is up to 40 m as seen from seismic sections. Gong et al. (2012, 2015) interpret that the sediment waves are mainly the product of oceanic bottom currents and modulated by sediment gravity flows. Kuang et al. (2014) interpret these sediment wavefields as a result of downslope moving turbidity currents. Alternatively, we interpreted that the sediment waves in the study area most likely result primarily from sediment gravity flows originated from the Tainan Slope or the

overbanking turbidity currents from the Formosa Canyon or the Penghu Canyon, a view in line with Kuang et al. (2014). The direction of the downslope gravity flows can be determined by the bedform geometry and the upslope migration of the crest point of the sediment waves.

Seismic facies C: Chaotic reflection configuration

Chaotic seismic facies is widely observed in the deepwater northeastern SCS margin, and it appears as discontinuous and transparent because of mid to low
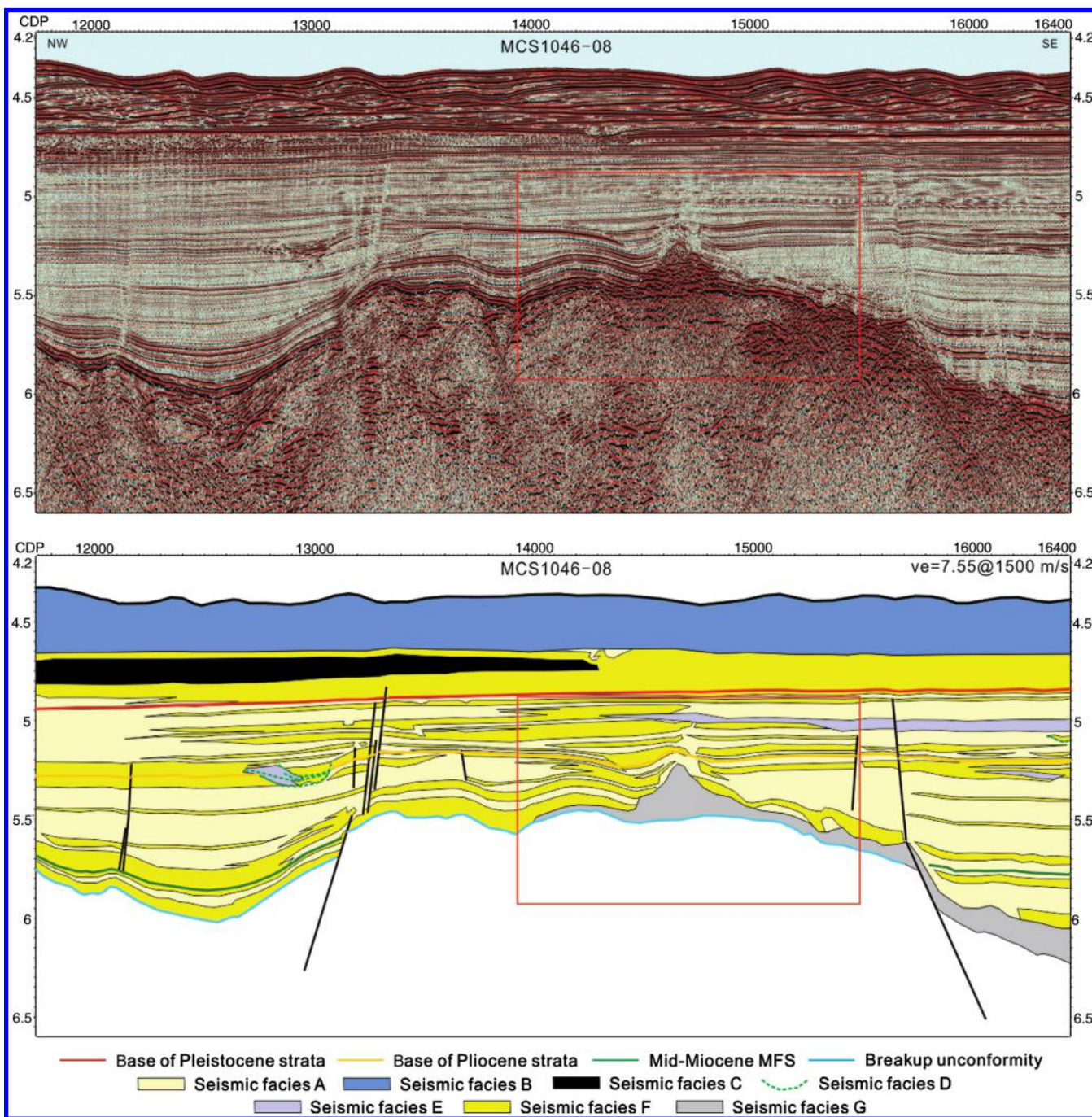

Figure 5. Seismic section and its interpretation of MCS1046-08, showing sediment waves and buried volcanic edifice near the Manila trench. The small buried volcano is characterized by seismic reflections of lava flows. Red rectangular displays the buried volcano and lava flows. Profile location is shown in Figure 2.

seismic amplitude. Seismic facies C exists predominantly in the Pliocene and Pleistocene strata along the base of slope (Figures 4, 5, 7, and 8) and in the canyon cut-and-fill features (Figures 3 and 8). It shows a spatially limited and sheetlike geometry in the canyon infills and a more widespread, irregular shape with erosional base in the Pliocene and Pleistocene strata along the base of slope. This seismic facies is interpreted as mass transport

deposits (MTDs) accumulated by sediment gravity flows or slide and slump processes.

Seismic facies D: U-shaped canyon-cut reflection configuration

U-shaped canyon-cut seismic facies mostly appears in late Miocene and Pliocene strata in the southeastern part of the study area (Figures 3 and 8). The U-shaped
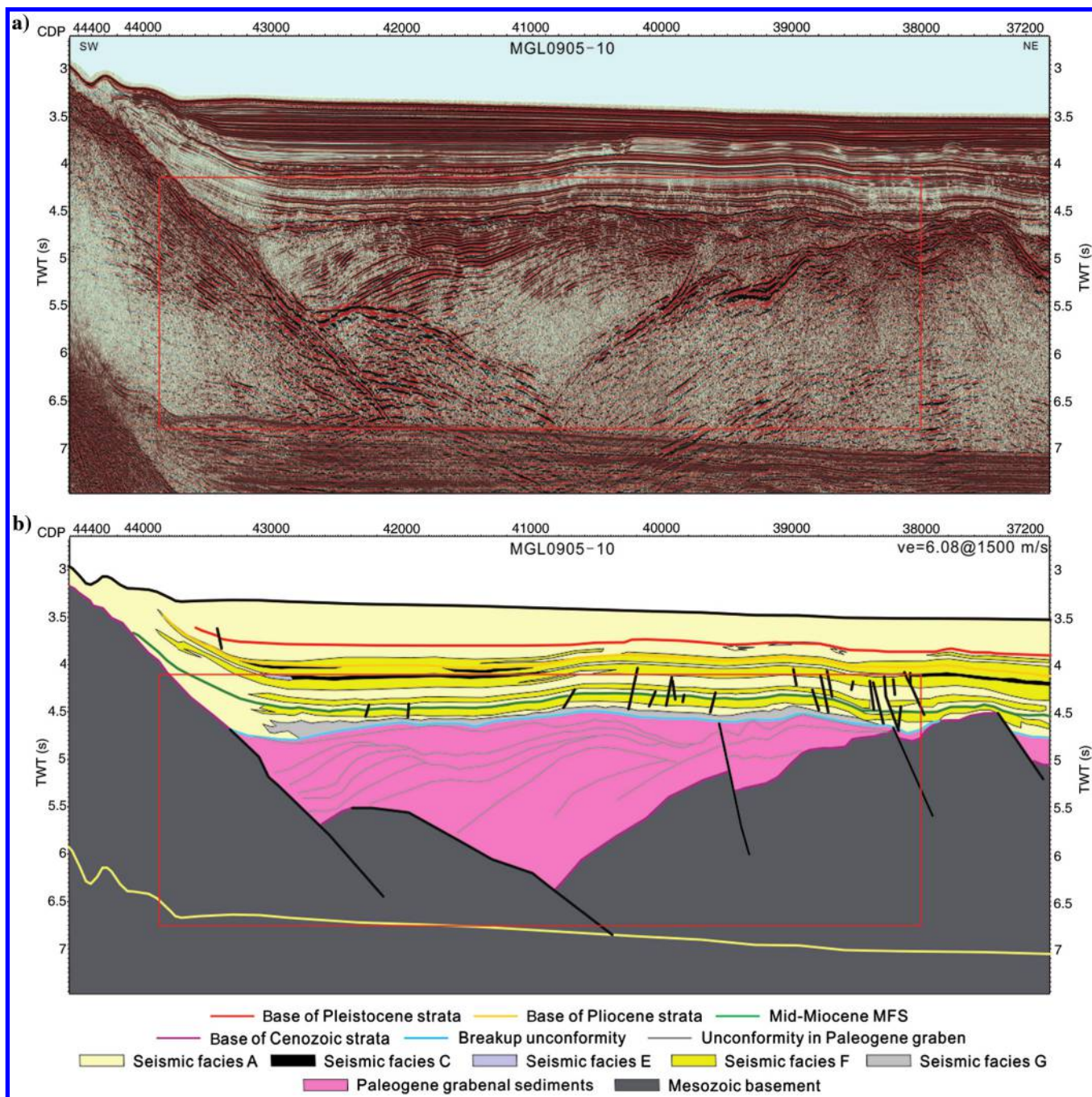
Figure 6. Seismic profile of MGL0905-10 showing grabens in the southwestern corner of the study area. Thin blue lines in the graben in (b) are the unconformities that are identified in the Paleogene graben. The Paleogene graben was resulted from rifting events with multiple normal faults. Red rectangle outlines the Paleogene graben. Profile location is shown in Figure 2.

canyon erosional surface cuts the strata up to 400 m deep with infill sediments characterized by interbedded MTD (seismic facies C) and turbidites (seismic facies F; see below). This seismic facies probably shows the entrenched channel or leveed channel of paleocanyons on the paleoslope.

Seismic facies E: Shingled reflection configuration

Seismic facies E of shingled reflections appears in the Miocene and Pliocene strata and encased in between more flat-lying layers in the western part of the study

area (Figures 5 and 7). However, a stacked series of multiple shingled layers exist beneath or near the modern Formosa Canyon. These shingled layers are interpreted as the lateral migrating and depositional bank of submarine channels.

Seismic facies F: HARP reflection configuration

The HARP seismic facies is typified by parallel, high-amplitude, continuous reflectors. It exists widely in the northern SCS margin with repeating occurrences (Figures 3–8). The total thickness of this seismic facies
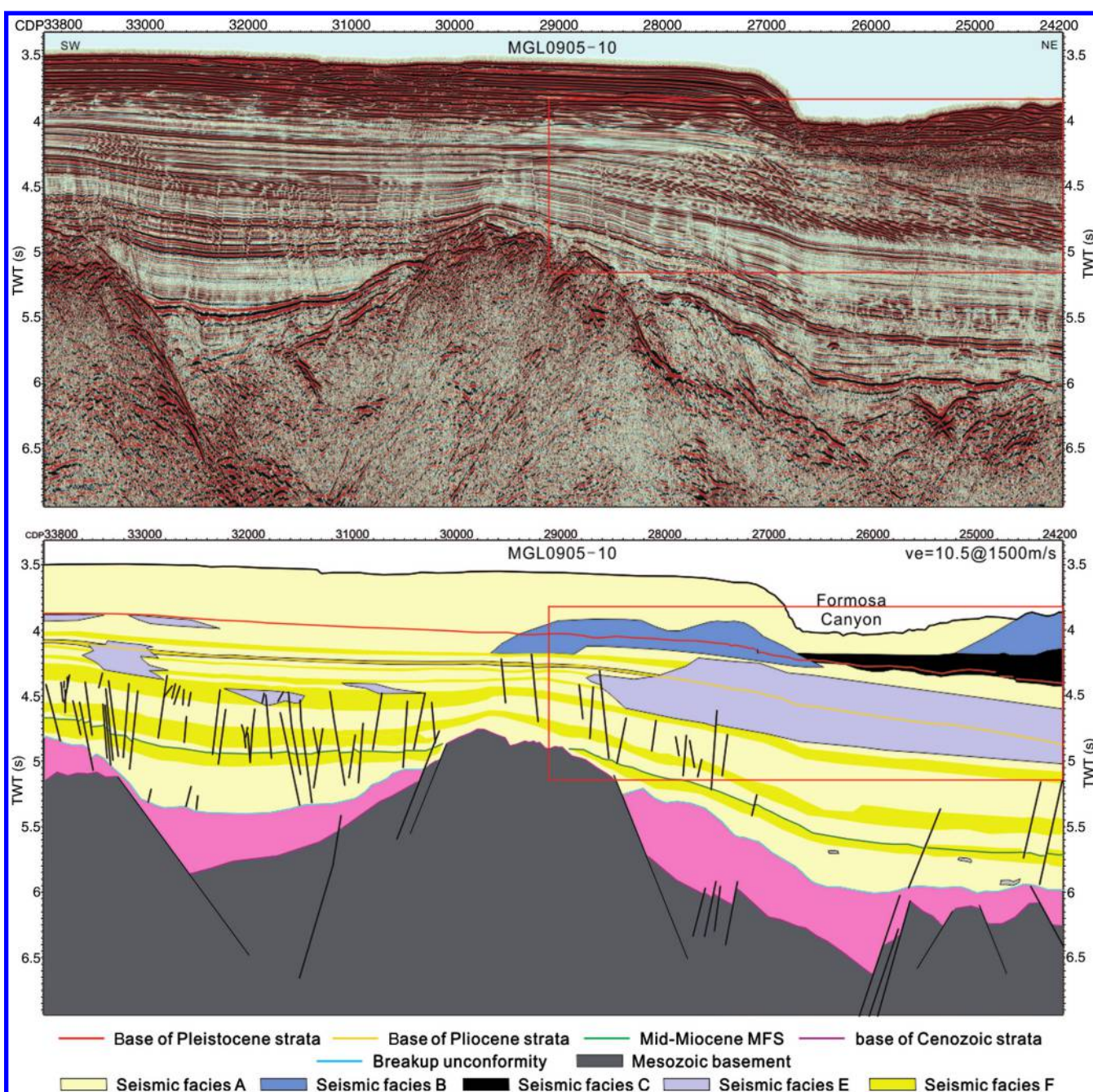

Figure 7. Seismic section and interpretation of MGL0905-10 showing features of lateral accretion and grabens in the central part of the study area. Lateral accretion features reveal development of paleochannels in this region during late Miocene. Red rectangle shows reflections interpreted as lateral accretions of channel. Profile location is shown in Figure 2.

in the eastern part of the study area is more than that in the western half. We interpreted this seismic facies as sheetlike turbidites brought about by frequent turbidity currents since the early Miocene.

Seismic facies G: Discontinuous, high-amplitude, and low-frequency reflection configuration

The reflection signature of this seismic facies generally appears as high-amplitude, discontinuous, and

low-frequency reflectors with some concave downward diffractions at the base (Figures 3–5). However, the transparency is very different in the emergent volcano group (Figure 3). The reflectors of emergent volcanos are characterized by very good transparency, whereas others reveal clear reflectors. This feature may be caused by the energy dissipation on the steep slope of the cone-shaped volcanic body. This seismic facies is interpreted as resulting from extrusive volcanics, lava flows, and volcanic sills.

Stratigraphic correlation

Four key stratal surfaces, the base of Pleistocene strata (approximately 1.8 Ma), the base of Pliocene strata (approximately 5.3 Ma), the mid-Miocene MFS (approximately 17 Ma), and the breakup unconformity are well-correlated in the rifted margin of the northeastern SCS (Figure 9). The northern depression, the central uplift zone, and a portion of the southern depression are developed beneath the shelf. The Oligocene-Miocene strata overlie directly above the Mesozoic basement in the central uplift zone and in the northern depression, whereas Paleogene syn-rift sediments are found in a Paleogene half-graben in the southern depression. A major half-graben of up to 2 s TWT in sediment thickness is found lying beneath the upper Tainan Slope (Li et al., 2007; Lester et al., 2012; Yeh et al., 2012, Figure 9). The footwall of the north-dipping graben bounding fault is a structural high, presumably underlain by Mesozoic sequences, which is directly covered by Quaternary sediments on its top (Figure 9). Within the graben infills key stratal surfaces and strata terminate against this graben bounding fault. Seismic characteristics of these key surfaces can still be correlated on both sides of this structural high, however (Figure 9).

In the deepwater area, reflectors for the base of Pleistocene and base of Pliocene are correlatable in most of the study area whereas reflectors for the mid-Miocene MFS and breakup unconformity cannot be correlated in some parts of the northern SCS margin (Figure 10). The distribution of spatially continuous Pliocene and Pleistocene bases indicates less tectonic activity during the Pliocene-Pleistocene. Disappearance of these two surfaces is only due to canyon erosion or due to a high-standing emergent volcano group (Figure 10). The Oligocene break-
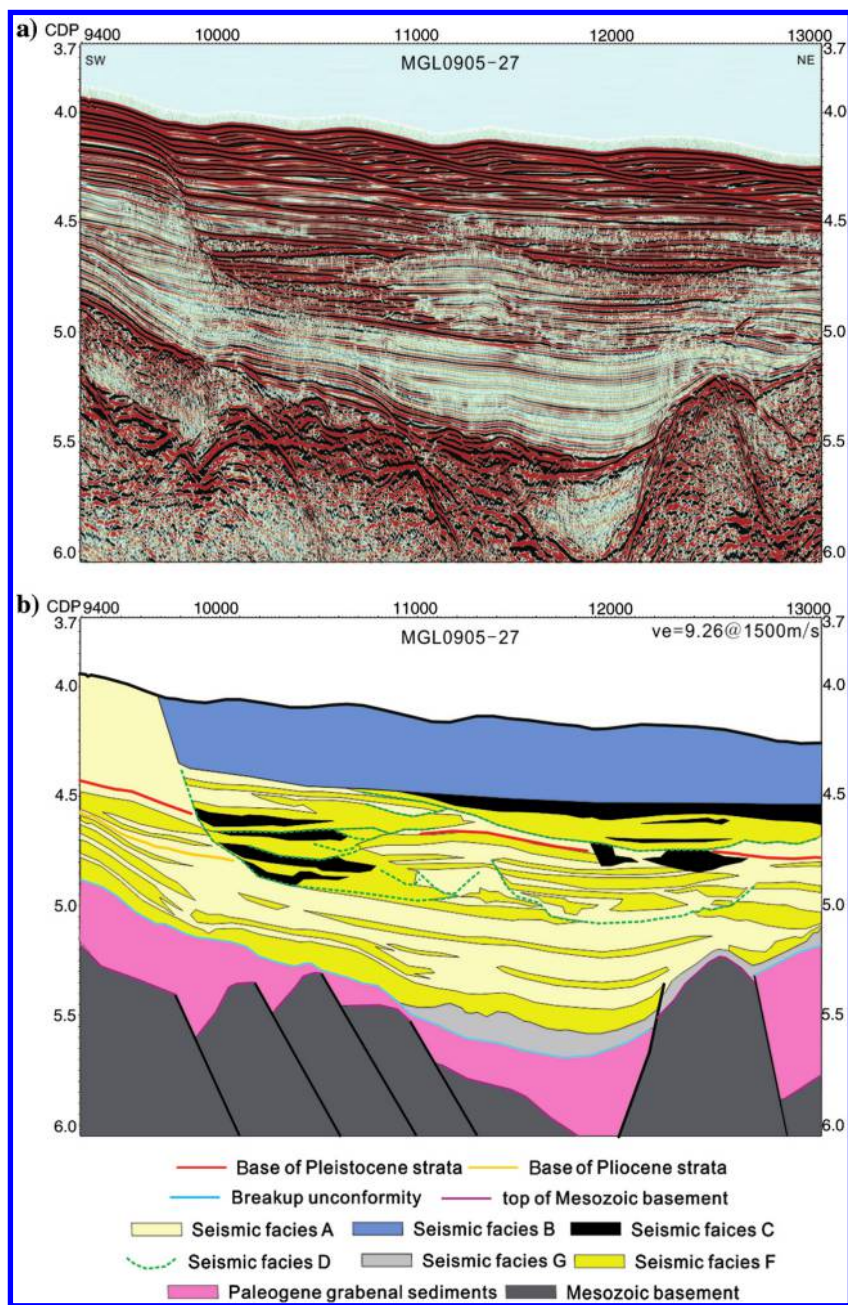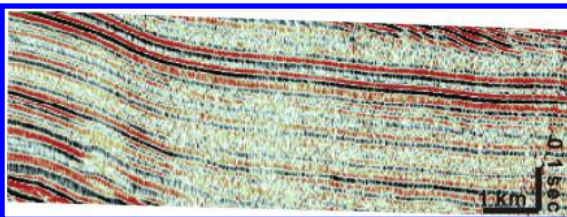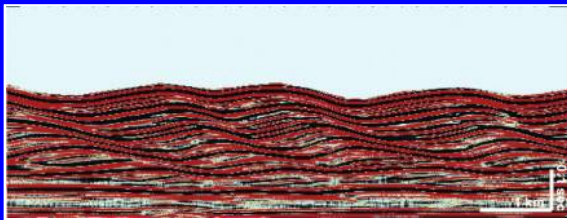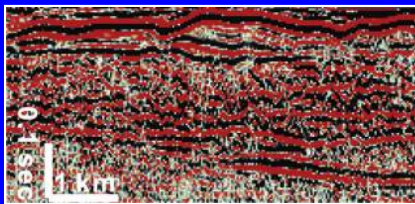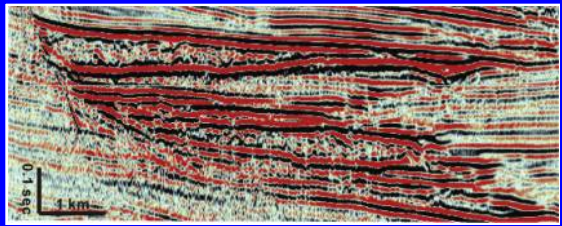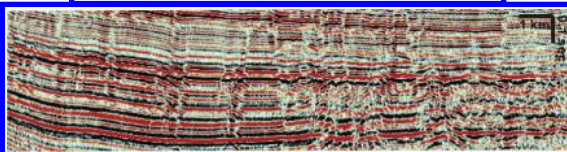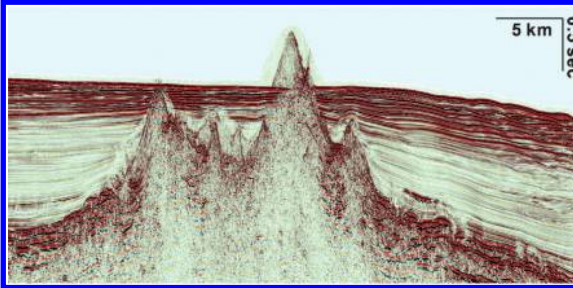

Figure 8. Seismic section of MGL0905-27 revealing the canyon cut-and-fill and sediment wave features in the eastern part of the study area. Panel (a) is uninterpreted profile and (b) is an interpreted section. Canyon-cut feature truncates the bases of Pliocene and Pleistocene bases with canyon fills showing HARP and chaotic seismic facies. Sediment waves lie above the base of Pleistocene. See Figure 2 for profile location.

up unconformity separates the underlying and tilted Paleogene syn-rift sediments from the overlying Neogene postbreakup strata (Figure 9). However, the breakup unconformity cannot be clearly identified in some parts of the northern SCS margin if the seismic data quality is poor.

Table 1. Description of seismic facies and their interpretation.

Seismic facies	Seismic expression	Interpretation	Example
Seismic facies A: Continuous and parallel reflection configuration	Parallel reflectors, intermediate to low amplitude, good continuity	Pelagic/hemiplegic sediments (low-amplitude reflections) interbedded with overbanking turbidites showing higher amplitude reflections	
Seismic facies B: Wavy and continuous reflection configuration	Wavy and high amplitude reflectors, good to intermediate continuity	Lateral migration and vertical accretion of deepwater sediment waves caused by oceanic bottom currents or sediment gravity flows	
Seismic facies C: Chaotic reflection configurations	Chaotic, low amplitude, discontinuous and uneven reflection signals	MTDs such as slumps and debris-flow deposits	
Seismic facies D: U-shaped canyon-cut reflection configuration	Abrupt termination of a series of reflections due to erosions	Submarine canyon incision and erosion	
Seismic facies E: Shingled reflection configuration	Shingled reflectors enclosed at its base and top by more gently dipping strata	Lateral accretion of the depositional flank of submarine channels	
Seismic facies F: HARP reflection configuration	Parallel/semiparallel, high-amplitude, and good continuity reflectors	Turbidites deposited in the channels or overbanking areas	
Seismic facies G: Discontinuous, high-amplitude, and low-frequency reflection configuration	High-amplitude and low-continuity reflectors, sometimes its top showing cone-shaped feature, refractions tend to occur at the base of rocks	Extrusive volcanics, lava flows, and sills related to extrusive volcanic activities	

Sediment thickness and sedimentation rates

The stratigraphic thicknesses are derived from the results of key stratal surface correlation. We performed a time-depth conversion using a velocity function obtained from hydrocarbon exploration wells in the Tainan shelf and the ODP Site 1148 in the SCS basin (Lin et al., 2014). The thicknesses and nominal sedimen-

tation rates for Pleistocene (1.8 Ma to present day), Pliocene (5.3–1.8 Ma), and middle to late Miocene (17–5.3 Ma) are calculated and shown in Figure 11. The results show that the areas with the thickest sediments (the depocenters) lie at the northeast corner of the study area since mid-Miocene. The stratigraphic thickness and averaged sedimentation rates for these
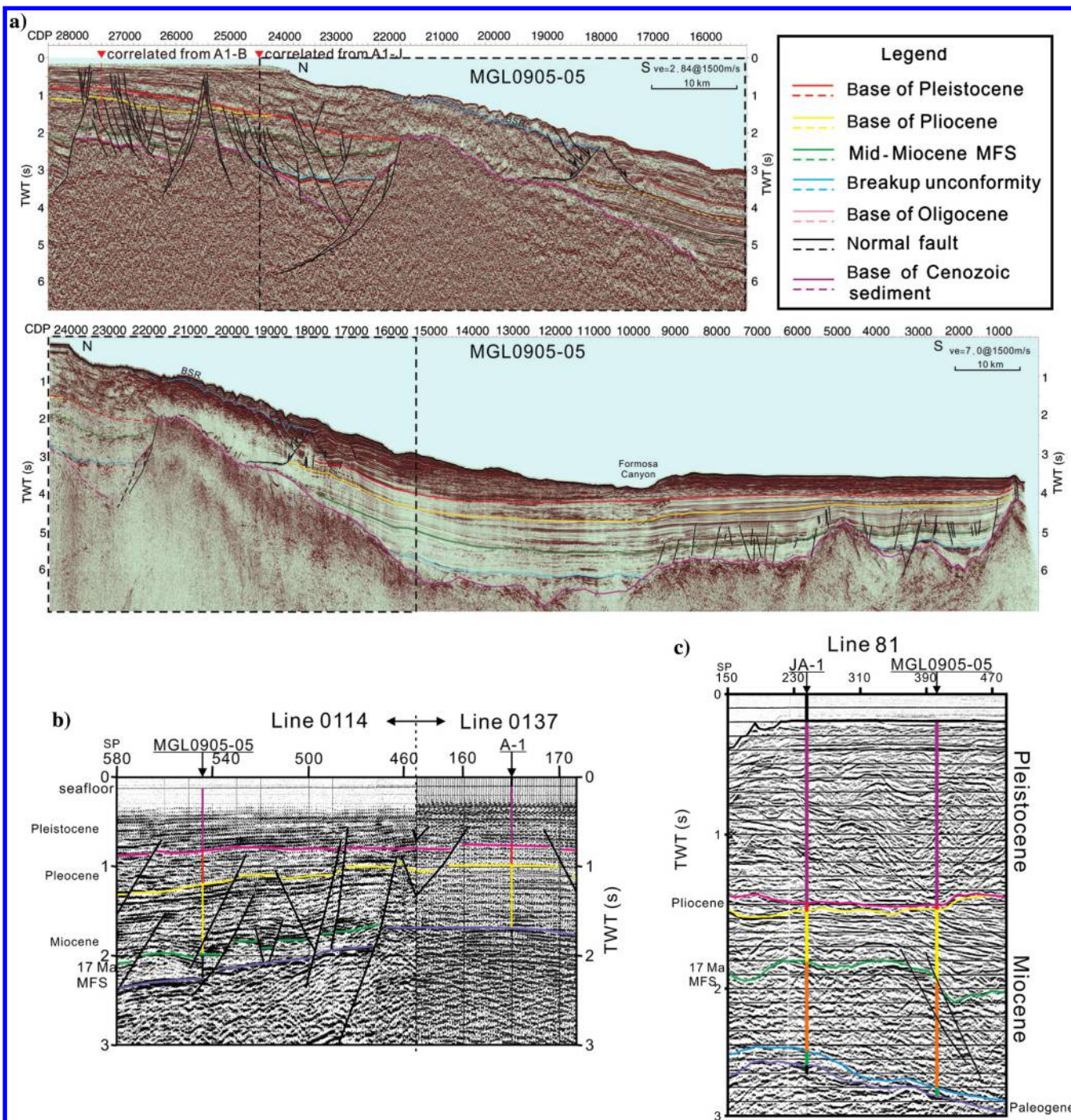

Figure 9. (a) Stratigraphic correlations on profile MGL0905-05 in the shelf to the deepwater region in the study area. Dashed rectangles in both panels show the same profiles. See Figure 2 for profile location of MGL0905-05. (b) Seismic stratigraphic correlation from borehole A-1 to MGL0905-05. (c) Seismic stratigraphic correlation from JA-1 borehole to MGL0905-05 section. Locations for these seismic lines and boreholes can be found in Figure 2.

three periods reveal different tectonic features. The middle to late Miocene strata thin southwardly, whereas the Plio-Pleistocene strata thins southwestwardly. The stratigraphic thickness and its thickness trend indicate that the northern SCS margin is probably a north–south-dipping continental slope during middle to late Miocene. In the Pliocene and the Pleistocene, the increasing sedimentation rate and clockwise-shifted thickness trend may indicate the influence of approaching Taiwan accretionary wedge and mountain belts.

Discussion
Cenozoic stratigraphy

Four key stratal surfaces have been correlated in the study area (Figure 9). These key seismic surfaces are correlated from the boreholes in the Tainan Basin
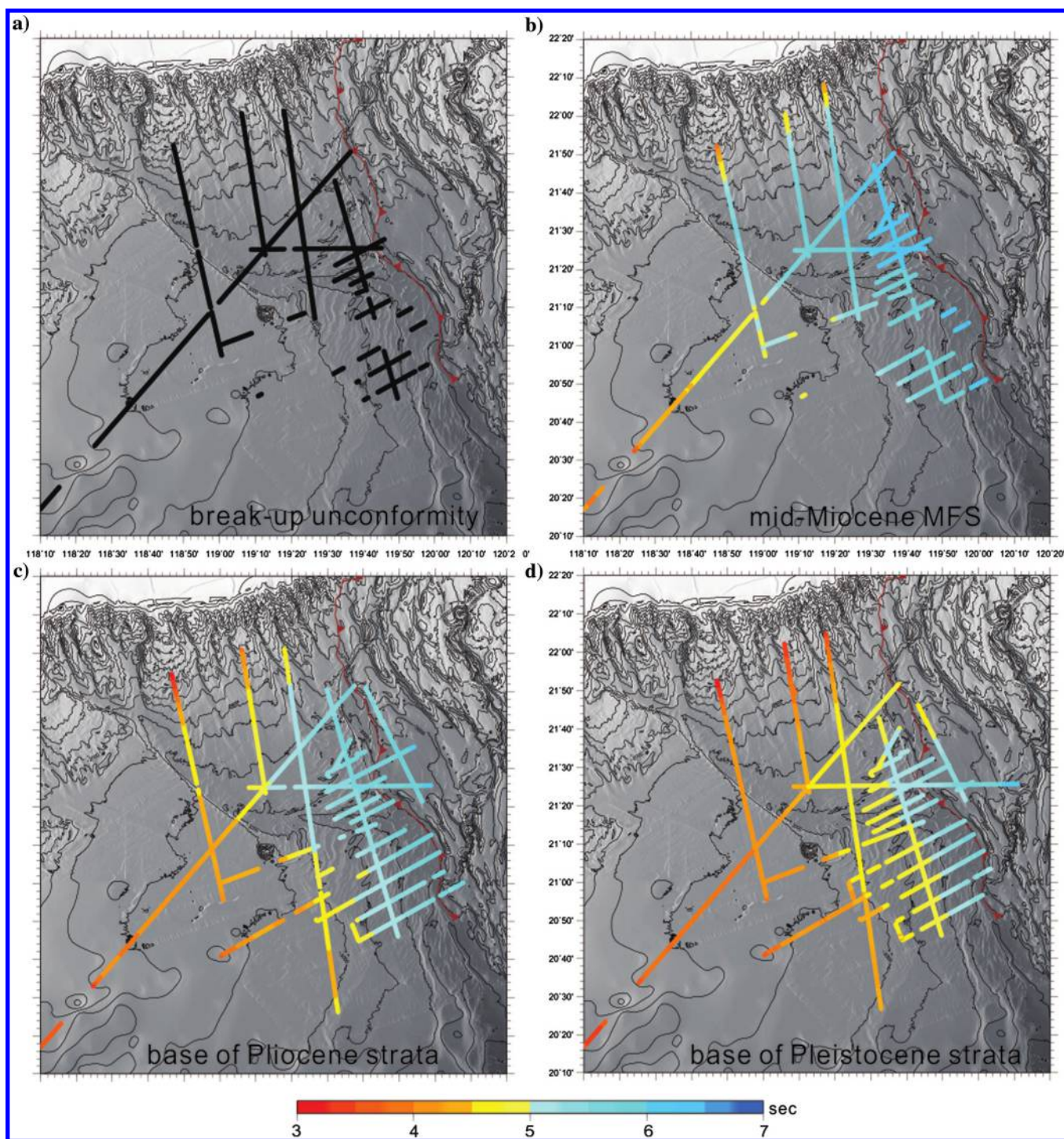

Figure 10. Color-coded line segments showing TWT of breakup unconformity (a), mid-Miocene MFS (b), base of Pliocene (c), and base of Pleistocene (d).

beneath the shelf (Figure 9) and from ODP drilling in the distal margin to the west of the study area (Figure 12). The Pleistocene sequence is characterized by strong seismic reflectivity, whereas the Pliocene sediments reveal weak reflectivity (Figures 9 and 12b). The middle to late Miocene strata show rather low-frequency features compared with the Pliocene sediments. The features of Pleistocene to upper Miocene sequences can be correlated with the sequence drilled at ODP Site 1148 (Li et al., 2015). The identification of these key stratigraphic horizons is similar to those by Li et al. (2007).

Paleogene grabens and underlying continental crust

The breakup unconformity divides the underlying Paleogene syn-rift sediments and the overlying late Oligocene to Recent postbreakup sequence beneath the Taiwan Strait (Lin et al., 2003). Stratigraphic correlations show that the breakup unconformity also exists in the deepwater area of the rifted continental margin. This key surface is also present in the western part of the northern SCS margin as seen on TAIGER seismic data

(e.g., Figure 10 of Lester et al. [2014] and Figure 4 of McIntosh et al. [2014]). The Paleogene grabens (Figures 6–8) developed on the top of the Mesozoic basement are well-identified on the seismic profiles. The rift geometry indicates episodic rifting activities during the Paleogene (Figure 6). Paleogene-rifted grabens developed in the northern SCS margin show a characteristic continental crust beneath the margin, indicating that the margin is a rifted continental margin rather than floored by oceanic crust. Recent studies also suggested shallower Moho beneath this area and indicated a thinned continental crust beneath the rifted continental margin (Lester et al., 2014; McIntosh et al., 2014).

Early postbreakup extrusive volcanic events

Seismic interpretation reveals many groups of volcanic bodies, shown as emergent or buried seamounts, lava flows, and sills developed in the deepwater area of the northern SCS margin (Figures 3, 5, and 6). There should be conduits for lava injecting from deep mantle through the rifted crust to shallow sub-bottom near the seafloor (Figures 3 and 4). However, the quality of our seismic data is not good enough to observe features related to magmatic dikes and vent complexes. We suggest that the postbreakup extrusive volcanic activities occurred in early Miocene and ceased to be active in mid-Miocene by the following pieces of evidence: (1) lava flows and sills are observed beneath the stratal surface of mid-Miocene MFS (17 Ma). Although the extrusive volcanic bodies are covered by the mid-Miocene MFS in the deepwater area, lava flows and sills are also buried by early Miocene sediments (Figures 3–5). (2) Age datings from an emergent volcano reveal that the volcanics were erupted approximately 21–22 Ma (Wang et al., 2012). The volcano group may develop since early postbreakup at approximately 30 to 21–22 Ma in age. The features of buried seamounts, lava flows, and volcanic sills in the southern part of the northern SCS margin near the Penghu Canyon/Manila Trench are consistent with the features of the emergent volcano group. This suggests that extensive extrusive volcanism occurred in the northern SCS margin during early postbreakup and probably ceased to be active by the end of the early Miocene Epoch. In the shelfal Tainan Basin and southern Taiwan mountain belts, postbreakup basaltic rocks are mostly early to middle Miocene in age (Sung et al., 2000) with the rare exception of late Miocene occurrences, such as some basalts in the Penghu island (Juang and Chen, 1992). The ages of igneous activ-
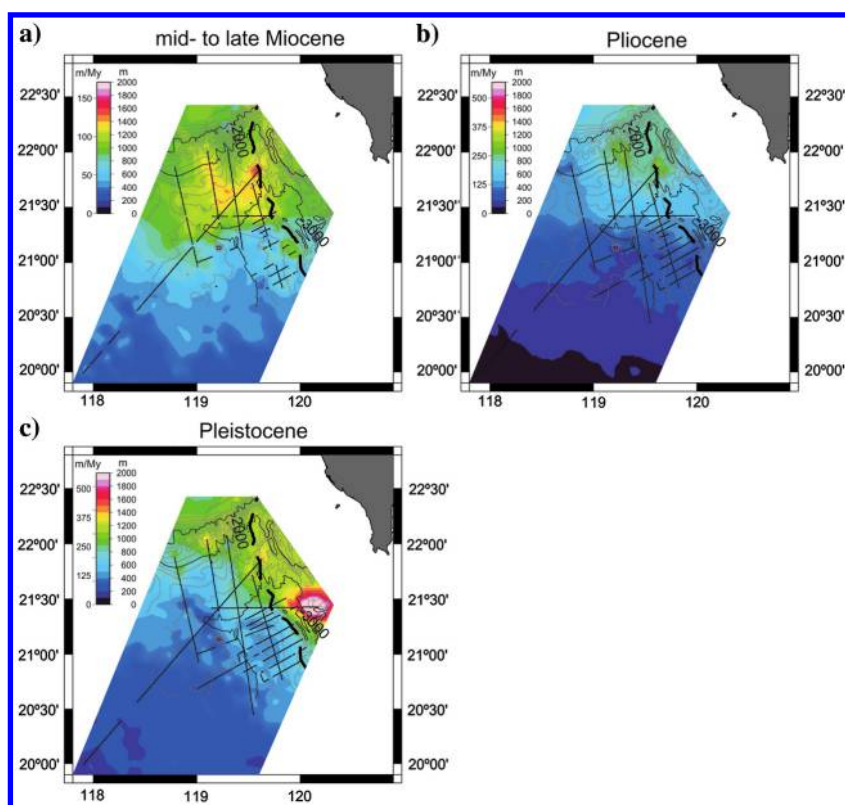

Figure 11. (a) Sediment thicknesses and averaged sedimentation rates during middle to late Miocene (17–5.3 Ma), (b) Pliocene (5.3–1.8 Ma), and (c) Pleistocene (1.8 Ma to present-day). The trend of the thickness (magnitude shown on the right side of scale bar) and the averaged sedimentation rate (magnitude shown on the left side of scale bar) reveal a shelf-break perpendicular trend during mid- to late Miocene and a clockwise-shifting trend during the Pliocene and Pleistocene. This feature probably shows the Taiwan Orogen developing at northeast of study area since the Pliocene epoch. Thin black lines are locations of interpreted seismic profiles. The thick black dashed line shows the deformation front of Taiwan accretionary wedge.

ities in our study area are in agreement with our suggestion for the postbreakup extrusive volcanic activity was active being primarily during early Miocene and probably ceased to be active in mid-Miocene.

Formosa canyon system and sediment waves

Canyon features, including lateral accretion and canyon cut-and-fill, are evident in the Neogene strata (Figures 3, 7, and 8). Seismic data show that the largest canyon system lies beneath or near the modern Formosa Canyon. The canyon infill is characterized by seismic facies E, indicating lateral accretion in the western part of the northern SCS margin, and showing as a proximal paleocontinental slope. In the eastern half of the study area, the canyon base erodes into the upper Miocene strata, indicating that the canyon has developed after the late Miocene (Figure 8). The canyon infills are characterized by interbedded strata of chaotic and HARP seismic facies (Figure 8), suggesting that large amounts of sandy sediments are accumulated in the canyon. The canyon cut-and-fill feature reveals developments of a submarine fan, leveed channels, and entrenched channels, relating to base-level changes on the lower continental slope during late Miocene and Pliocene.

Two sediment wavefields of distinct morphologic features are observed lying to the west of modern deformation front/Manila Trench and to the north and south of Formosa Canyon, respectively. These two sediment wavefields are classified by their wavelengths and seismic reflection patterns (Gong et al., 2012, 2015; Kuang et al., 2014). The base of the sediment wavefields

in northern SCS margin shows that these fields have developed since early to middle Pleistocene (Figures 4, 6, and 8). Some sediment wavefields are buried or found outside of the aforementioned sediment wavefields in the northern SCS margin (Figures 3 and 7). These sediment wave strata may have started their development in late Pliocene or early Pleistocene. The sediment wavefields are mainly originated from downslope-moving supercritical turbidity currents (Kuang et al., 2014; Zhong et al., 2015).

Tectonic development of the Cenozoic rifted margin

Our stratigraphic correlation and seismic interpretation help to outline the tectonic and sedimentary features in the northern SCS continental margin offshore southwest Taiwan (Figure 13). Before the oceanic spreading of the SCS commenced at approximately 30 or 33 Ma (Barckhausen et al., 2014), continental rifting resulted in a series of normal faults with horst-and-graben features (Figure 13). The grabens were filled with syn-rift sediments. A half-graben is observed to lie beneath the Jiulong Ridge in the Tainan Slope (Lester et al., 2012; Liao et al., 2014) for example. Seismic-facies analyses indicate that early postrift sediments, which overlie the breakup unconformity, are all deepwater facies (see Figures and 6, 7, 8, 9, and 12). This indicates that there was a phase of rapid tectonic subsidence following the continental breakup or incipient seafloor spreading at 30 or 34 Ma. This phase of early postrift rapid subsidence during the late Oligocene to early Miocene is observed in the Tainan Basin (Lin et al., 2003), and it is interpreted
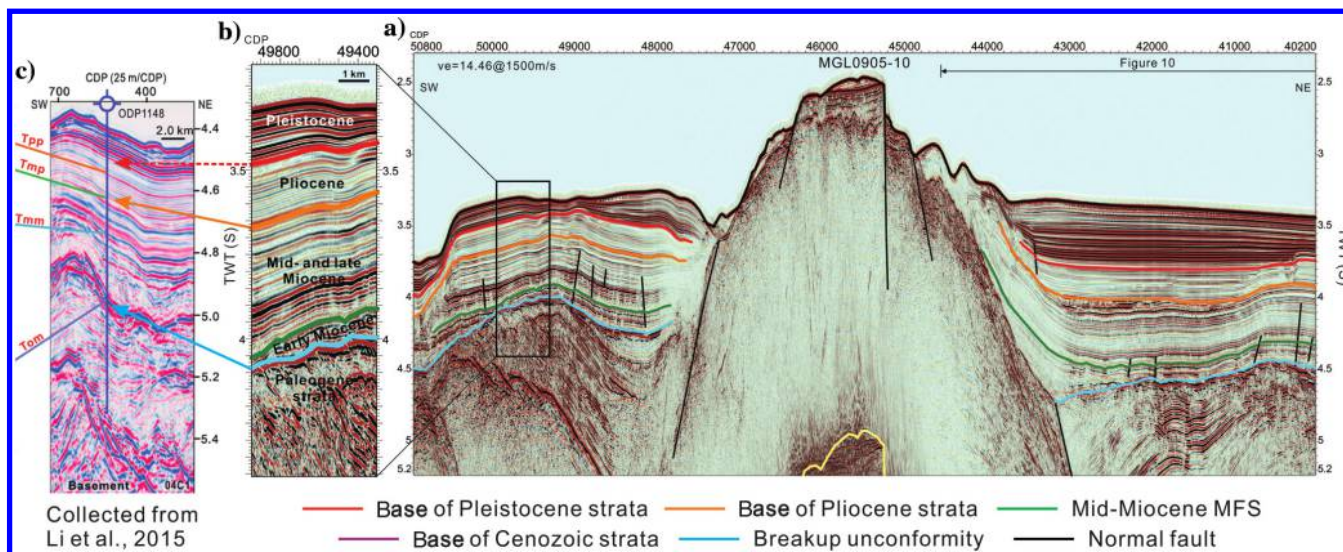

Figure 12. (a) Seismic sections and stratigraphics correlations between MGL0905-10 (this study) and seismic section crossing ODP Site 1148 (c) as reported in Li et al. (2015). Seismic facies can be well-correlated on both sides of basement high shown in MGL-0905-10. Profile location is shown in Figure 2. (b) A magnified seismic section showing seismic features to the southwest of the basement high. Key stratal surfaces and characteristics for each sequence can be easily observed in this section. (c) Seismic section showing features of Cenozoic sequences crossing ODP Site 1148. The surface, Tpp (Pliocene-Pleistocene boundary, 2.58 Ma), in (c) is based on new Geological Time Scale 2012 (Gradstein et al., 2012), whereas the base of Pleistocene strata in this study followed old definition of base of Pleistocene (1.8 Ma) as reported in the well-completion reports of boreholes A-1 and JA-1 (see Fig. 2).

to result from rapid cooling from a thermal perturbation during late syn-rift stage (Lin et al., 2003). This hypothesis was later supported by numerical modeling (Shi et al., 2008). In view of the breakup unconformity being always covered immediately by deepwater facies and the suggested rapid tectonic subsidence during the early postrift phase, we interpret that the rate of tectonic subsidence increases rapidly toward the distal rifted margin. Therefore, a sigmoidal bathymetric profile has developed since the early postbreakup stage. Postbreakup extrusive volcanic activity was vigorous in the early Miocene, leading to the development of many groups of extrusive volcanos in the southern part of the northeast SCS margin (Figure 13). The extrusive volcanic activities largely ceased to be active by middle Miocene. Formosa Canyon system started to develop by late Miocene. The drainage of the Formosa Canyon may be obstructed by the distribution of extrusive volcanic bodies or buried seamounts (Figure 13). During the Pliocene, the central uplift zone of the Tainan Basin was an isolated high (probably a shallow and submerged area or subaerially exposed, Tzeng et al., 1996). Sandy sediments were blocked by this high and the Formosa Canyon served as the main sediment conduit to transport terrestrial and coarse-grained sediments to the deep sea. Submarine fans may develop in the distal part of the study area

(Figure 13) with sediments delivered from the Formosa Canyon and perhaps other canyons from the northeast of the margin. In response to the westward advance of the Taiwan orogenic/accretionary wedge during the Pleistocene, flexural normal faults started to develop near the Manila Trench due to plate flexure for the subducting plate. The sediment wavefields also started to develop in the early or middle Pleistocene (Figure 13). In the late Pleistocene, Formosa Canyon drainage shifted eastward and converged into the Manila Trench (Figure 13).

Conclusions

A Cenozoic tectonic and sedimentary development model in the rifted northern continental margin of the SCS near Taiwan is proposed by integrating reflection seismic and borehole data. The conclusions of this study are as follows:

1) The stratigraphic correlation from the shelf reveals that four key stratal surfaces, the base of Pleistocene, base of Pliocene, mid-Miocene MFS, and breakup unconformity, are well-correlated in the northeast SCS. The reflection pattern of the Pleistocene, Pliocene, and late Miocene sediments can also be consistently correlated with those observed at ODP site 1148.

2) The spatial distribution of stratigraphic thicknesses and averaged sedimentation rates derived from seismic stratigraphic correlations indicate the paleogeography and depocenters for each period. The northern SCS margin is a southeast-dipping continental slope during middle to late Miocene, whereas the clockwise-shifted thickness trend indicates the influence of Taiwan accretionary wedge during the Pliocene and Pleistocene when the accretionary wedge gradually approaching the study area.

3) The northeast SCS margin off southwest Taiwan develops on a rifted and thinned continental crust. Many features, such as Paleogene grabens and graben bounding faults, and the shallower Moho surface in the southern part of the northern SCS margin as reported in the literature, suggest the nature of the continental crust beneath the distal margin.

4) The margin is dominated by horst and graben due to continental rifting before the SCS oceanic spreading. The breakup unconformity separates the underlying syn-rift sediments and the overlying postbreakup strata. Extrusive volcanic activity was vigo-
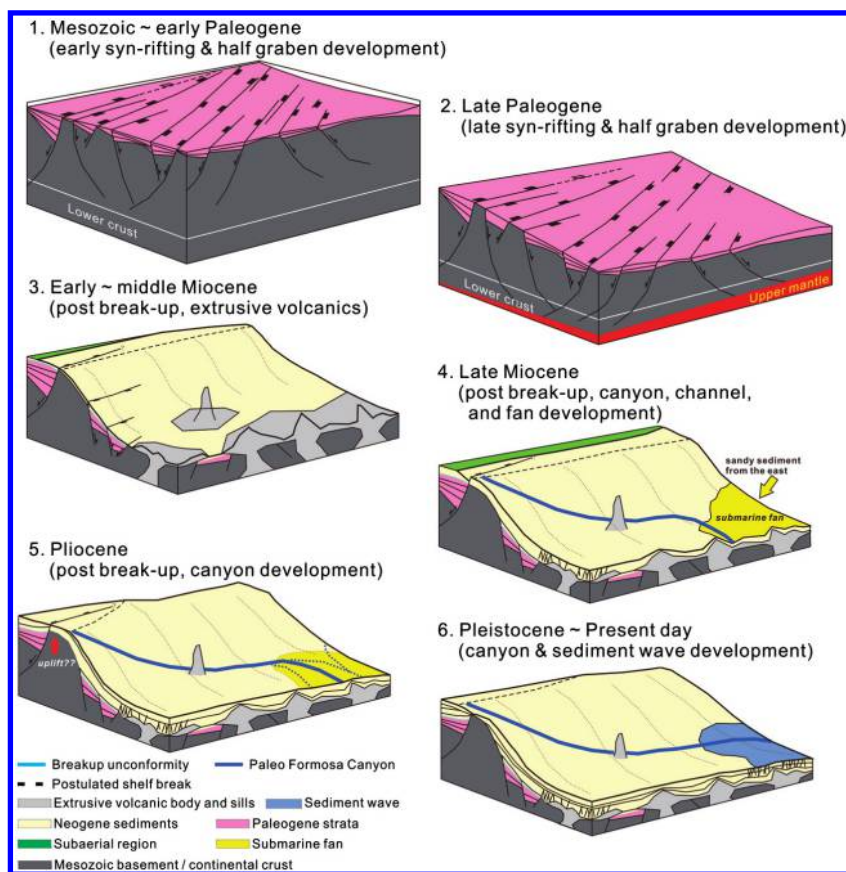

Figure 13. Schematic drawings showing the Cenozoic tectonic and sedimentary development of the northern SCS continental margin in the study area.

rous in the early Miocene and probably ceased to be active by middle Miocene. Formosa Canyon started to develop in late Miocene and gradually evolved to the modern configuration. Submarine fans may have developed in the southeastern margin during the Pliocene. Finally, two sediment wavefields have developed since early or middle Pleistocene.

Acknowledgments

References

Barckhausen, U., E. Martin, D. Franke, S. Ladage, and M. Pubellier, 2014, Evolution of the South China Sea: Revised ages for breakup and seafloor spreading: Marine and Petroleum Geology, **58**, 599–611, doi: 10.1016/j.marpetgeo.2014.02.022.

Briais, A., P. Patriat, and P. Tapponnier, 1993, Updated interpretation of magnetic anomalies and seafloor spreading stages in the South China Sea: Implications for the Tertiary tectonics of Southeast Asia, Journal of Geophysical Research, **98**, 6299–6328, doi: 10.1029/92JB02280.

Catuneanu, O., 2006, Principles of sequence stratigraphy: Elsevier.

Chen, L, W. C. Chi, S. K. Wu, C. S. Liu, C. T. Shyu, Y. Wang, and C. Y. Lu, 2014, Two dimensional fluid flow models at two gas hydrate sites offshore southwestern Taiwan: Journal of Asian Earth Sciences, **92**, 45–253.

Damuth, J. E., 1979, Migrating sediment waves created by turbidity currents in the northern South China Basin: Geology, **7**, 520–523, doi: 10.1130/0091-7613(1979)7<520: MSWCBT>2.0.CO;2.

Ediger, V., A. F. Velegrakis, and G. Evans, 2002, Upper slope sediment waves in the Cilician Basin, northeastern Mediterranean: Marine Geology, **192**, 321–333.

Gong, C., Y. Wang, X. Peng, W. Li, Y. Qiu, and S. Xu, 2012, Sediment waves on the South China Sea Slope off southwestern Taiwan: Implications for the intrusion of the Northern Pacific Deep Water into the South China Sea: Marine and Petroleum Geology, **32**, 95–109.

Gong, C., Y. Wang, S. Xu, K. T. Pickering, X. Peng, W. Li, and Q. Yan, 2015, The northeastern South China Sea margin created by the combined action of down-slope and along-slope processes: Processes, products and implications for exploration and paleoceanography: Marine and Petroleum Geology, **64**, 233–249.

Gradstein, F. M., J. G. Ogg, M. D. Schmitz, and G. M. Ogg (coordinators), 2012, The Geologic Time Scale 2012 2: Elsevier, Boston, plus chart, 1176.

Hsu, S. K., Y. C. Yeh, W. B. Doo, and C. H. Tsai, 2004, New bathymetry and magnetic lineations identifications in the northernmost South China Sea and their tectonic implications: Marine Geophysical Researches, **25**, 29–44, doi: 10.1007/s11001-005-0731-7.

Juang, W. S., and J. C. Chen, 1992, Geochronology and geochemistry of Penghu basalts, Taiwan Strait and their tectonic significance: Journal Southeast Asian Earth Sciences, **7**, 185–193, doi: 10.1016/0743-9547(92)90053-E.

Kuang, Z., G. Zhong, L. Wang, and Y. Guo, 2014, Channel-related sediment waves on the eastern slope offshore Dongsha Islands, northern South China Sea: Journal of Asian Earth Sciences, **79**, 540–551, doi: 10.1016/j.jseaes.2012.09.025.

Lee, T. Y., C. H. Tang, J. S. Ting, and Y. Y. Hsu, 1993, Sequence stratigraphy of the Tainan Basin, offshore southwestern Taiwan: Petroleum Geology of Taiwan, **28**, 119–158.

Lester, R., L. L. Lavier, K. McIntosh, H. J. A. Van Avendonk, and F. Wu, 2012, Active extension in Taiwan's precollision zone — A new model of plate bending in continental crust: Geology, **40**, 831–834, doi: 10.1130/G33142.1.

Lester, R., H. Van Avendonk, K. McIntosh, L. Lavier, C. S. Liu, T. K. Wang, and F. Wu, 2014, Rifting and magmatism in the northeastern South China Sea from wide-angle tomography and seismic reflection imaging: Journal of Geophysical Research — Solid Earth, **119**, 2305–2323, doi: 10.1002/2013JB010639.

Lewis, K. B., and H. M. Pantin, 2002, Channel-axis, overbank and drift sediment waves in the southern Hikurangi Trough, New Zealand: Marine Geology, **192**, 123–151, doi: 10.1016/S0025-3227(02)00552-2.

Li, X. H., 2000, Cretaceous magmatism and lithospheric extension in Southeast China: Journal of Asian Earth Sciences, **18**, 293–305, doi: 10.1016/S1367-9120(99)00060-7.

Li, C. F., J. Li, W. Ding, D. Franke, Y. Yao, H. Shi, X. Pang, Y. Cao, J. Lin, D. K. Kulhanek, T. Willams, R. Bao, A. Briais, E. A. Brown, Y. Chen, P. D. Clift, F. S. Colwell, K. A. Dadd, I. Hernandez-Almeida, Z. L. Huang, S. Hyun, T. Jiang, A. A. P. Koppers, Q. Li, C. Liu, Q. Liu, Z. Liu, R. H. Nagai, A. Peleo-Alampay, X. Su, Z. Sun, M. L. G. Tejada, H. S. Trinh, Y. C. Yeh, C. Zhang, F. Zhang, G. L. Zhang, and X. Zhao, 2015, Seismic stratigraphy of the central South China Sea basin and implications for neotectonics: Journal of Geophysics Research — Solid Earth, **120**, doi: 10.1002/2014JB011686.

Li, C. F., Z. Zhou, J. Li, H. Hao, and J. Geng, 2007, Structures of the northeasternmost South China Sea continental margin and ocean basin — Geophysical constraints and tectonic implications: Marine Geophysical Researches, **28**, 59–79, doi: 10.1007/s11001-007-9014-9.

Liao, W. Z., A. T. Lin, C. S. Liu, J. N. Oung, and Y. Wang, 2014, Heat flow in the rifted continental margin of the South China Sea near Taiwan and its tectonic implications: Journal of Asian Earth Sciences, **92**, 233–244, doi: 10.1016/j.jseaes.2014.01.003.

Lin, A. T., 2001, Cenozoic stratigraphy and Tectonic development of the West Taiwan Basins: Ph.D. thesis, University of Oxford.

Lin, A. T., A. B. Watts, and S.P. Hesselbo, 2003, Cenozoic stratigraphy and subsidence history of the South China Sea margin in the Taiwan region: Basin Research, **15**, 453–478, doi: 10.1046/j.1365-2117.2003.00215.x.

Lin, C. C., A. T. Lin, C. S. Liu, C. S. Horng, G. Y. Chen, and Y. Wang, 2014, Canyon-infilling and gas hydrate occurrences in the frontal fold of the offshore accretionary wedge off southern Taiwan: Marine Geophysical Researches, **35**, 21–35, doi: 10.1007/s11001-013-9203-7.

Lin, A. T., C. S. Liu, C. C. Lin, P. Schnurle, G. Y. Chen, W. Z. Liao, L. S. Teng, H.-J. Chuang, and M.-S. Wu, 2008, Tectonic features associated with the overriding of an accretionary wedge on top of a rifted continental margin — An example from Taiwan: Marine Geology, **255**, 186–203, doi: 10.1016/j.margeo.2008.10.002.

Lom-Keil, H. V., V. Spiess, and V. Hopfauf, 2002, Fine-grained sediment waves on the western flank of the Zapiola Drift, Argentine Basin — Evidence for variations in Late Quaternary bottom flow activity: Marine Geology, **192**, 239–258, doi: 10.1016/S0025-3227(02)00557-1.

Ludmann, T, H. K. Wong, and P. Wang, 2001, Plio-Quaternary sedimentation processes and neotectonics of the northern continental margin of the South China Sea: Marine Geology, **172**, 331–358, doi: 10.1016/S0025-3227(00)00129-8.

Ludman, T., and H. K. Wong, 1999, Neotectonic regime on the passive continental margin of the northern South China Sea: Tectonophysics, **311**, 113–138, doi: 10.1016/S0040-1951(99)00155-9.

McIntosh, K, H. Van Avendonk, L. Lavier, R. Lester, D. Eakin, F. Wu, C. S. Liu, and C. S. Lee, 2013, Inversion of a hyper-extended rifted margin in the southern Central Range of Taiwan: Geology, **41**, 871–874, doi: 10.1130/G34402.1.

McIntosh, K., L. Lavier, H. Van Avendonk, R. Lester, D. Eakin, and C. S. Liu, 2014, Crustal structure and inferred rifting processes in the northeast South China Sea: Marine and Petroleum geology, **58**, 612–626, doi: 10.1016/j.marpetgeo.2014.03.012.

Mosher, D. C., and R. E. Tomson, 2002, The Foreslope Hills: Large-scale, fine-grained sediment waves in the Strait of Georgia, British Columbia: Marine Geology, **192**, 275–295, doi: 10.1016/S0025-3227(02)00559-5.

Nissen, S. S, D. E. Hayes, P. Buhl, J. Diebold, B. Yao, W. Zeng, and Y. Chen, 1995, Deep penetrating seismic sounding across the northern margin of the South China Sea: Journal of Geophysical Research — Solid Earth, **100**, 22407–22433, doi: 10.1029/95JB01866.

Shi, X., H. Xu, X. Qiu, K. Xia, X. Yang, and Y. Li, 2008, Numerical modeling on the relationship between thermal uplift and subsequent rapid subsidence: Discussions on the evolution of the Tainan Basin: Tectonics, **27**, TC6018, doi: 10.1029/2007TC002163.

Sibuet, J. C., S. K. Hsu, X. Le Pichon, J. P. Le Formal, D. Reed, G. Moore, and C. S. Liu, 2002, East Asia plate tectonics since 15 Ma — Constraints from the Taiwan region: Tectonophysics, **344**, 103–134, doi: 10.1016/S0040-1951(01)00202-5.

Sung, Q., C. W. Lin, W. H. Lin, and W. C. Lin, 2000, Explanatory text of the geological map of Taiwan (scale 1:50, 000) Sheet 51: Chiahsien: Central Geological Survey, Ministry of Economic Affairs.

Tang, F. S., J. N. Oung, Y. Y. Hsu, and C. N. Yang, 1999, Elementary study of structural evolution in Tainan Basin in southwest Taiwan Strait (in Chinese): Petroleum Geology of Taiwan, **33**, 125–149.

Taylor, B., and D. E. Hayes, 1983, Origin and history of the South China Sea Basin, *in* C. E. Hayes (ed.), The tectonic and geologic evolution of Southeast Asian Seas and Islands 2: American Geophysical Union, Geophysical monograph **27**, 23–56.

Tsao, W. C. Q., J. N. Oung, C. M. Yang, Y. W. Lee, M. H. Wang, Y. C. Uang, and S.-L. Tang, 1992, Studies on hydrocarbon potential of Mesozoic formation in the Tainan Basin, southwestern offshore Taiwan (in Chinese): Journal of Mining and Metallurgy, **36**, 32–45.

Tzeng, J., Y. C. Uang, Y. Y. Hsu, and L. S. Teng, 1996, Seismic stratigraphy of the Tainan Basin (in Chinese): Petroleum Geology of Taiwan, **30**, 281–308.

Wang, K. L., Y. M. Lo, S. L. Chung, C. H. Lo, S. K. Hsu, H. J. Yang, and R. Shinjo, 2012, Age and geochemical features of dredged basalts from offshore SW Taiwan — The coincidence of intra-plate magmatism with the spreading South China Sea: Terrestrial, Atmospheric and Oceanic Sciences, **23**, 657–669.

Wynn, R. B., and D. A. V. Stow, 2002, Classification and characterization of deepwater sediment waves: Marine Geology, **192**, 7–22, doi: 10.1016/S0025-3227(02)00547-9.

Yang, K. M., H. H. Ting, and J. Yuan, 1991, Structural styles and tectonic models of Neogene extensional tectonics in southwestern Taiwan — Implications for hydrocarbon exploration: Petroleum Geology of Taiwan, **26**, 1–31.

Yeh, Y. C., J. C. Sibuet, S. K. Hsu, and C. S. Liu, 2010, Tectonic evolution of the Northeastern South China Sea from seismic interpretation: Journal of Geophysical Research — Solid Earth, **115**, B06103, doi: 10.1029/2009JB006354.

Yeh, Y. C., S. K. Hsu, W. B. Doo, J. C. Sibuet, C. S. Liu, and C. S. Lee, 2012, Crustal features of the northeastern South China Sea — Insights from seismic and magnetic interpretations: Marine Geophysical Research, **33**, 307–326, doi: 10.1007/s11001-012-9154-4.

Zhong, G., M. J. B. Cartigny, Z. Kuang, and L. Wang, 2015, Cyclic steps along the South Taiwan Shoal and West Penghu submarine canyons on the northeastern continental slope of the South China Sea: Geological Society of America Bulletin, **127**, 804–824, doi: 10.1130/B31003.1.

Wei-Zhi Liao received a Ph.D. (2015) from the Department of Earth Sciences, National Central University, Taiwan. He has been a postdoctoral fellow at the Institute of Oceanography, National Taiwan University since late 2015. His research interests include the fields of tectonics, sedimentary processes, and basin analysis.

Biographies and photographs of the other authors are not available.